Energy Proceedings
Vol 53, 2025
ISSN 2004-2965

Research on Vehicle Thermal Management Control Strategy for Fuel Cell Vehicles under High-temperature Conditions Based on Model Predictive Control#

Huitao Zhang, Fengxiang Chen *, Yaowang Pei
School of Automotive Studies, Tongji University, Shanghai 201804, China
(Corresponding Author: fxchen@tongji.edu.cn)

ABSTRACT

To ensure the safety of fuel cell vehicles and enhance overall vehicle performance, comprehensive thermal management is essential. Currently, thermal management for fuel cell vehicles mainly focuses on low-temperature environments, with relatively little research on high-temperature conditions. This paper proposes an integrated vehicle thermal management solution that includes thermal management for the fuel cell, lithium-ion battery, motor, and cabin. Additionally, a vehicle thermal management system model is built and the control strategies for high-temperature conditions are developed. Model predictive control algorithm is designed to settle down the air conditioning system cooling both the cabin and the lithium-ion battery in high-temperature environments. Simulation results demonstrate that this comprehensive thermal management solution exhibits excellent temperature control capabilities under extreme high-temperature conditions with lithium-ion battery response time of 2324s and cabin response time of 60.13s. And lithium-ion battery temperature is robust to variations of cabin temperature. Additionally, the temperatures of the fuel cell and motor are effectively controlled within the reference range.

Keywords: Model Predictive Control, Fuel cell vehicles, Vehicle thermal management, Automotive air conditioning.

NONMENCLATURE

Abbreviations	
FCEV	Fuel Cell Electric Vehicles
TMS	Thermal Management System
LDV	Flow distribution value
TXV	Thermal expansion valve
PEMFC	Proton exchange membrane fuel cell
ITMS	Integrated thermal management systems
MPC	Model Predictive Controller
PID	Proportional-Integral-Derivative
Symbols	
P	Power[W]
m	Mass [kg]
V	Volume [m^3]
ρ	Density [kg m^{-3}]
g	Gravitational acceleration [m s-^{2}]
C	Resistance
A	Area [m^2]
T	Temperature [K]
$\dot{m}$	Mass flow rate [kg s^{-1}]
h	Enthalpy [J/kg]
η	Efficiency [%]
Q	Heat generate rate [W]

1 INTRODUCTION

In recent years, with the continuous development of industrial technology, energy and environmental issues have gradually emerged[1]. Fuel cell vehicles are gradually gaining widespread adoption due to their exceptional energy efficiency and environmental friendliness[2]. To ensure stable operation of vehicles and enhance their overall economy and power performance, thermal management of the entire vehicle is necessary. Su et al.[3] proposed an ITMS which can meet the cooling requirements of the fuel cell and the motor under heavy load conditions, but it does not consider the cooling of the cabin and the lithium-ion battery. Xu et al.[4] proposed a TMS that can meet the cooling requirements of all components; however, this system does not consider the utilization of waste heat from the fuel cell and the motor. Considering the utilization of waste heat from the fuel cell, Lee et al.[5] employed a heat pump system to utilize the waste heat from the PEMFC. However, this system does not take high-temperature conditions into account.

This is a paper for the 16th International Conference on Applied Energy (ICAE2024), Sep. 1-5, 2024, Niigata, Japan.

To address thermal management issues under different temperatures, an ITMS has been proposed. Taking into account the characteristics of ITMS in which air conditioning cools both the cabin and the lithium-ion battery under high-temperature conditions. MPC is designed to control the FDV opening and the air conditioning compressor speed.

2 MODEL OF FUEL CELL VEHICLE

The structure of the FCEV system is shown in Fig. 1. PEMFC is connected to the bus through a DC/DC converter. PEMFC and Lithium-ion battery meet power demands according to different operating conditions, where PEMFC and Lithium-ion battery high-frequency and low-frequency electrical energy respectively. Lithium-ion battery is charged when vehicle brakes. FCEV model parameters are shown in Table 1.

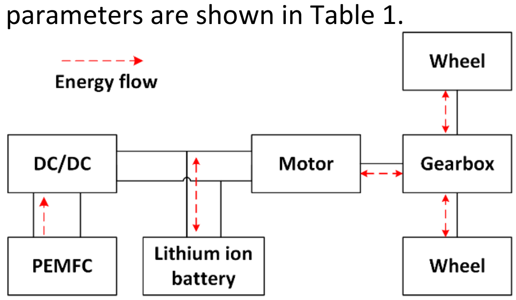

Fig. 1 Structure of the fuel cell vehicle powertrain

Table 1 FCEV model parameters

Parameters	Value
Vehicle overall weight	$m = 2150\text{kg}$
Aerodynamic drag coefficient	$C_d = 0.33$
Tire rolling resistance coefficient	$C_{roll} = 0.0072$
Tire radius	$r = 0.365\text{m}$
Vehicle frontal area	$A_{front} = 2.75\text{m}^2$
Battery pack capacity	29 kWh
Motor specific heat capacity	$cp_{EM} = 880\ \text{J kg}^{-1}\ \text{K}^{-1}$
Motor mass	$M_{EM} = 58\ \text{kg}$
Stack specific heat capacity	$cp_{st} = 500\text{J kg}^{-1}\ \text{K}^{-1}$
Stack mass	$M_{st} = 45\text{kg}$
Coolant specific heat capacity	$cp_{cool} = 3600\ \text{J kg}^{-1}\ \text{K}^{-1}$
Internal resistance of lithium-ion battery	$R_{int} = 0.06\ \Omega$
Lithium-ion battery mass	$m_{bat} = 160\ \text{kg}$
Compressor volumetric efficiency	$\eta_{comp,vol} = 0.85$
Refrigerant density	$\rho_{rfg} = 10.03\ \text{kg m}^{-3}$
Compressor displacement	$V_{comp} = 50\ \text{ml}$

2.1 Vehicle dynamics model

The power of the whole vehicle can be obtained from the equilibrium equation of driving force and driving resistance[6]

$$P_{req} = \left(C_{roll} mg\cos\theta + mg\sin\theta + \frac{1}{2}\rho_{air} C_d A_{front} v^2 + \sigma m\dot{v} \right) v \quad (1)$$

where P_{req} is power of the whole vehicle[W], , θ is slope angle[°], ρ_{air} is air density[kg m^{-3}], v is vehicle speed[m s^{-1}], σ is conversion factor for rotational mass, $\dot{v}$ is vehicle acceleration[m s^{-2}].

2.2 Thermal Management System

The TMS of a fuel cell vehicle is capable of precisely controlling the temperature of key components such as the fuel cell stack, motor, and lithium-ion battery, which enhances energy conversion efficiency and system stability. Additionally, it ensures a comfortable cabin temperature under different ambient temperatures.

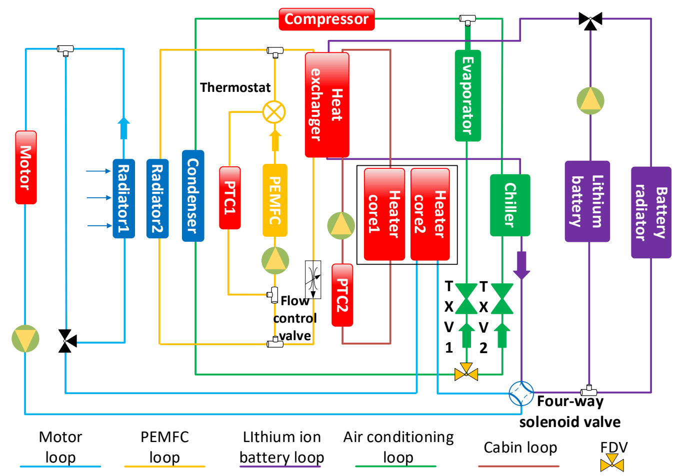

Fig. 2 Thermal management system of FCEV

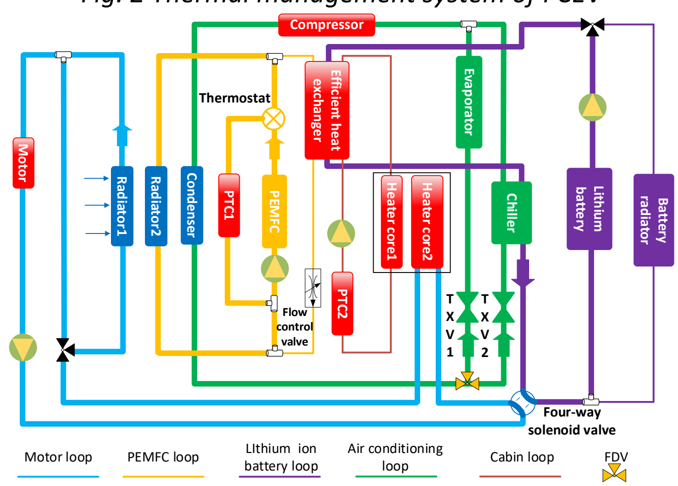

Fig. 3 ITMS under high-temperature conditions

An ITMS is proposed in this paper, as shown in Fig. 2. It has a simple and compact structure, ensuring that all components operate at their optimal working temperatures under different ambient temperatures.

The model of the ITMS under high-temperature conditions is shown in Fig. 3. Fuel cell and motor dissipate heat separately, while lithium-ion battery and cabin are cooled through the air conditioning system.

2.2.1 Motor thermal management loop

The power of motor is defined as

$$P_{EM} = \frac{P_{req}}{\eta_{EM2w}} \tag{2}$$

where η_{EM2w} is the efficiency from the motor to the wheels.

$$Q_{EM} = \begin{cases} \frac{P_{EM}}{\eta_m} - P_{EM}, \text{drive} \\ P_{EM} - P_{EM} \cdot \eta_m, \text{brake} \end{cases} \tag{3}$$

where η_m is the efficiency of the motor [%], which can be obtained by checking the torque and speed table. The motor efficiency diagram is shown in Fig. 4.

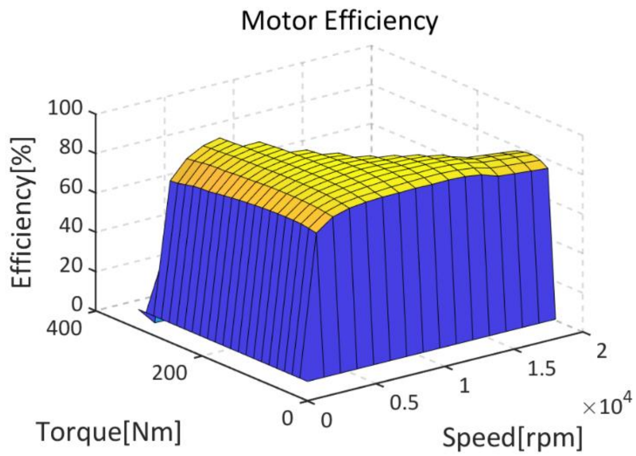

Fig. 4 Motor efficiency diagram

The dynamic temperature change process of the motor is described as

$$cp_{EM} M_{EM} \frac{dT_{EM}}{dt} = Q_{EM} + h_{EM,cool} A_{EM,cool} \left(T_{EM,cool}^{out} - T_{EM} \right) \tag{4}$$

where T_{EM} is the motor temperature [K], $T_{EM,cool}^{out}$ is outlet coolant temperature of the motor [K], $T_{EM,cool}$ is the coolant temperature within the motor [K], and $\dot{m}_{EM,col}$ is mass flow rate of the coolant flowing through the motor [kg s^{-1}].

2.2.2 PEMFC thermal management loop

The model of the fuel cell thermal management loop is calculated by

$$cp_{st} M_{st} \frac{dT_{st}}{dt} = Q_{FC} + k_{st} \left(T_{st,cool}^{out} - T_{st} \right) \tag{5}$$

where T_{st} is the stack temperature[K], k_{st} is the convective heat transfer coefficient [J K^{-1}], $T_{st,cool}^{out}$ is the outlet coolant temperature of the stack [K], $T_{st,cool}$ is the coolant temperature inside the stack [K], and $\dot{m}_{st,col}$ is the mass flow rate of the coolant flowing through the stack [kg s^{-1}][7]. The major and minor loops are modeled according to the reference[8].

2.2.3 Lithium-ion battery thermal management loop

The heating power of the lithium-ion battery is calculated by

$$Q_{bat} = I^2 R_{int} \tag{6}$$

The dynamic changes in the temperature of the lithium-ion battery is described as

$$m_{bat} cp_{bat} \frac{dT_{bat}}{dt} = Q_{bat} + h_{bat,cool} A_{bat,cool} (T_{bat,cool} - T_{bat}) \tag{7}$$

where T_{bat} is the lithium-ion battery temperature [K], and $T_{bat,cool}$ is the temperature of the coolant inside the lithium-ion battery [K].

The high-temperature coolant flowing out of the lithium-ion battery exchanges heat with the low-temperature refrigerant in the chiller. The mass flow rate of the refrigerant $\dot{m}_{chill,rfg}$ in the chiller equals the total mass flow rate of the refrigerant minus the mass flow rate of the refrigerant in the evaporator $\dot{m}_{evap,rfg}$

$$\begin{cases} \dot{m}_{chill,rfg} = \dot{m}_{cond,rfg} - \dot{m}_{evap,rfg} \\ \dot{m}_{evap,rfg} = \dot{m}_{cond,rfg} \gamma \end{cases} \tag{8}$$

where γ is the opening of LDV.

2.2.4 Air conditioning refrigeration loop

In the air conditioning refrigeration loop, the mass flow rate of the refrigerant at the compressor outlet and the outlet enthalpy are calculated by

$$\dot{m}_{rfg} = \frac{\eta_{comp,vol} N_{comp} \rho_{rfg} V_{comp}}{60 \times 10^6} \tag{9}$$

$$h_{comp,rfg}^{out} = h_{comp,rfg}^{in} + (h_{comp,rfg}^{out*} - h_{comp,rfg}^{in}) / \eta_p \tag{10}$$

where N_{comp} is the compressor speed [rpm], $h_{comp,rfg}^{in}$ is the enthalpy of the refrigerant at the compressor inlet [kJ/kg], and $h_{comp,rfg}^{out*}$ is the enthalpy at the compressor outlet during adiabatic compression [kJ/kg], η_p is isentropic efficiency of compressor[%].

After the high-temperature refrigerant exits the air conditioner compressor, it enters the condenser where it condenses into a liquid refrigerant. The dynamic changes in the refrigerant, the condenser wall, and the surrounding environment temperatures in the condenser are described as

$$m_{cond,rfg}\frac{dh_{cond,rfg}}{dt}=\dot{m}_{cond,rfg}\left(h_{cond,rfg}^{in}-h_{cond,rfg}^{out}\right)+h_{cond,rfg,w}A_{cond,rfg,w}\left(T_{cond,w}-T_{cond,rfg}\right) \tag{11}$$

$$m_{cond,w}cp_{cond,w}\frac{dT_{cond,w}}{dt}=-h_{cond,rfg,w}A_{cond,rfg,w}\left(T_{cond,w}-T_{cond,rfg}\right)-h_{cond,air,w}A_{cond,air,w}\left(T_{cond,w}-T_{cond,air}\right) \tag{12}$$

$$m_{cond,air}cp_{cond,air}\frac{dT_{cond,air}}{dt}=h_{cond,air,w}A_{cond,air,w}(T_{cond,w}-T_{cond,air})+\dot{m}_{cond,air}cp_{cond,air}(T_{cond,air}^{in}-T_{cond,air}^{out}) \tag{13}$$

where $h_{cond,rfg}$ is the enthalpy of the refrigerant in the condenser [kj kg^{-1}], $h_{cond,rfg}^{in}$ and $h_{cond,rfg}^{out}$ are the enthalpies of the refrigerant at the inlet and outlet of the condenser [kj kg^{-1}], $T_{cond,w}$ is the condenser wall temperature [K], $T_{cond,rfg}$ is the refrigerant temperature inside the condenser [K], $T_{cond,air}$ is the ambient air temperature around the condenser [K], $\dot{m}_{cond,air}$ is the mass flow rate of air passing through the condenser [kg/s], $T_{cond,air}^{in}$ and $T_{cond,air}^{out}$ are the air temperatures before and after passing through the condenser [K], and $\dot{m}_{cond,rfg}$ is the mass flow rate of the refrigerant inside the condenser [kg s^{-1}]. The expansion valve is modeled according to the reference[9].

The dynamic process of cabin temperature changes is described as

$$m_{cab,air}cp_{air}\frac{dT_{cab}}{dt}=Q_{AC}+Q_{amb}+Q_p+Q_I \tag{14}$$

where T_{cab} is cabin temperature[K], Q_{AC} is the air conditioning cooling capacity[W], Q_{amb} is the heat transfer between the vehicle and the environment[W], Q_p is the metabolic heat production of the human body[W], and Q_I is the solar radiation[W][10].

3 MODEL PREDICTIVE CONTROL ALGORITHM DESIGN

The control algorithm for the ITMS is shown in Fig. 5. Air conditioning is required to cool both the lithium-ion battery and the cabin in high-temperature. Meanwhile, the motor and fuel cell are cooled using radiators. Therefore, the MPC algorithm is adopted in this paper to control the FDV opening γ and the air conditioning compressor speed N_{comp} to ensure the temperature of the cabin and the lithium-ion battery. PID controllers are adopted to control the motor loop water pump speed $N_{EM,pump}$, lithium-ion battery loop water pump speed $N_{bat,pump}$, PEMFC loop water pump speed $N_{st,pump}$, and thermostat opening α.

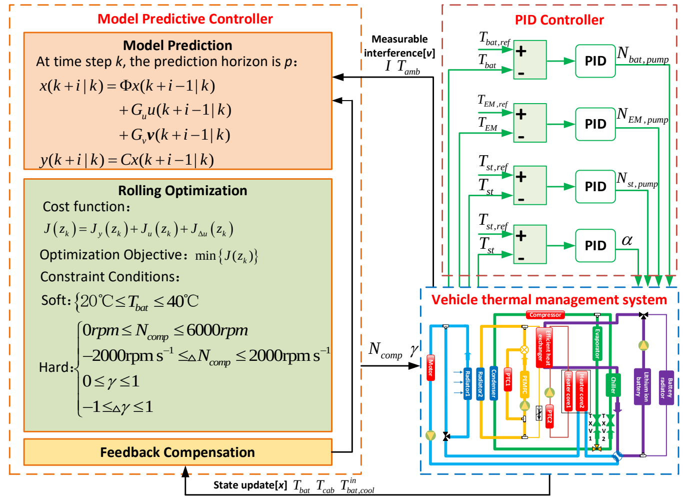

Fig. 5 The ITMS control Strategy

MPC possesses three core elements: Model Prediction, Rolling Optimization and Feedback Compensation.

1) Model Predictive

To reduce control complexity and enhance the robustness and stability of the control system, the dynamic model of lithium-ion battery temperature variation is simplified. When the vehicle operates, the output current of the lithium-ion battery is approximately 50A. Therefore, the model is linearized around I=50A, resulting in the state-space representation of the system as follows

$$\begin{cases}\dot{x}=Ax+B_u u+B_v v\\ y=Cx\end{cases} \tag{15}$$

where the state variable of the system are $x=[T_{bat},T_{bat,cool},T_{cab}]^T$, the control input are $u=[N_{comp},\gamma]^T$, the measurable disturbance are $v=[I,T_{amb}]^T$, and the system output are $y=[T_{bat},T_{cab}]^T$.

The state-space expression is discretized as follows

$$\begin{cases}x(k+1)=\Phi x(k)+G_u u(k)+G_v \mathbf{v}(k)\\ y(k+1)=Cx(k)\end{cases} \tag{16}$$

Given the small sampling period *T*, it can be approximated that $\Phi=I+TA$, $G_u=TB_u$, $\Phi=I+TA$, $G_u=TB_u$.

2) Rolling Optimization

The cost function used in this paper is defined as

$$J\left(z_k\right)=J_y\left(z_k\right)+J_u\left(z_k\right)+J_{\Delta u}\left(z_k\right) \tag{17}$$

where $J_y\left(z_k\right)$ reflects the deviation of the lithium-ion battery and cabin temperatures from their target values, $J_u\left(z_k\right)$ reflects the energy consumption associated with the control efforts, and $J_{\Delta u}\left(z_k\right)$ reflects the rate of change in the control inputs.

To ensure the practical feasibility of the control strategy, the following constraints are incorporated:

Hard constraints:

$$0rpm \le N_{comp} \le 6000rpm$$

$$-2000\text{rpm s}^{-1} \le \Delta N_{comp} \le 2000\text{rpm s}^{-1}$$

$$0 \le \gamma \le 1$$

$$-1 \le \Delta\gamma \le 1$$

Soft constraints:

$$20℃ < T_{bat} < 40℃$$

3) Feedback Compensation

By real-time monitoring of the actual temperatures of the lithium-ion battery and cabin, this information is utilized to revise and optimize the prediction results, enabling the system to more precisely approximate the desired control performance.

The controller parameters are shown in Table 2.

Table 2 Controller parameters

Parameter	Value
State space expression matrix	$A=\begin{bmatrix} -1.1\times10^{-3} & 9.9914\times10^{-4} & 0 \\ 8.88\times10^{-3} & -8.88\times10^{-3} & 0 \\ 0 & 0 & -3.31\times10^{-1} \end{bmatrix}$ $B_u=\begin{bmatrix} 0 & 0 \\ -7.0358\times10^{-5} & 1.6635 \\ -3.0944\times10^{-4} & -1.1448 \end{bmatrix}$ $B_v=\begin{bmatrix} 3.6397\times10^{-5} & 1.4276\times10^{-4} \\ 0 & 0 \\ 0 & 3.313\times10^{-1} \end{bmatrix}$ $C=\begin{bmatrix} 1 & 0 & 0 \\ 0 & 0 & 1 \end{bmatrix}$

4 SIMULATION ANALYSIS

Parameters of simulation model and controller are shown in Table 1 and Table 2.

To validate the control performance of the algorithm at high-temperature, simulations are conducted under an ambient temperature of 40°C. The actual vehicle speed and the reference speed are illustrated in Fig. 6(a), while the power demands for the entire vehicle, the fuel cell, and the lithium-ion battery are presented in Fig. 6(b), (c), and (d), respectively.

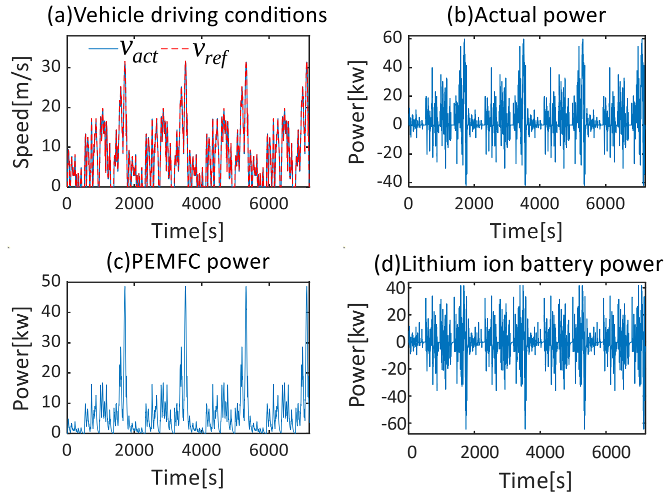

Fig. 6 Vehicle operating conditions and comprehensive power demand of power sources: (a) Vehicle operating conditions; (b) Total vehicle power demand; (c) Fuel cell power demand; (d) Lithium-ion battery power demand.

Fig. 6 (a) illustrates that the actual vehicle operating conditions are essentially the same as the reference conditions, indicating that the vehicle meets the expected driving conditions. The total vehicle power demand fluctuates between positive and negative values, with positive power indicating driving and negative power indicating braking, which can be explained in Fig. 6(b).

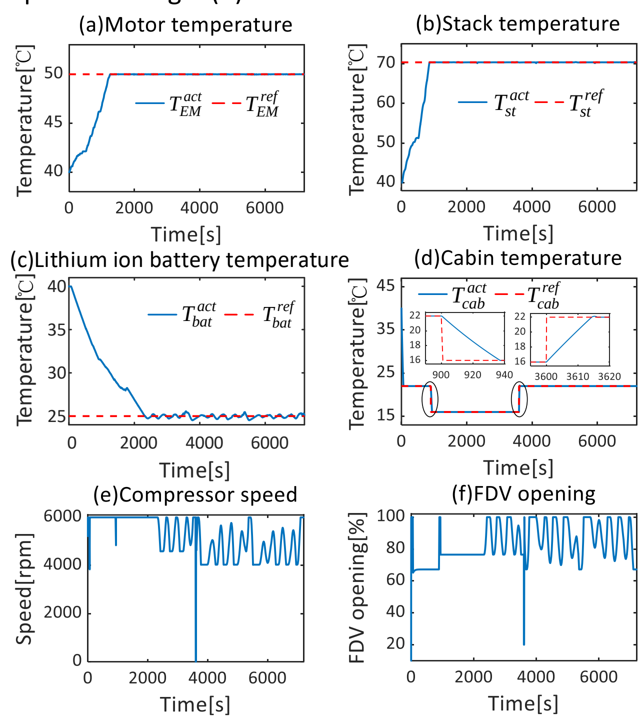

Fig. 7 Simulation results of MPC for ITMS: (a) Motor temperature, (b) PEMFC stack temperature, (c) Lithium-ion battery temperature, (d) Cabin temperature, (e) Compressor speed, (f) FDV opening.

The simulation results of MPC for ITMS under high-temperature are shown in Fig. 7. The motor temperature variation is shown in Fig. 7(a). As the vehicle operates, the motor temperature rose from 40°C and started dissipating heat upon reaching 50°C, maintaining the temperature at 50°C. Fig. 7(b) shows the stack temperature variation which indicates that the stack temperature remained essentially at the reference temperature. Fig. 7(c) and (d) show that the MPC algorithm has good control performance. The lithium-ion battery temperature decreased from 40°C and reached the reference temperature with response time of 2324 seconds, as shown in Fig. 7(c). The cabin temperature reached the reference temperature with response time of 60.13 seconds, which can be explained in Fig. 7(c). Considering the possibility of the driver adjusting the cabin reference temperature, variations of cabin reference temperature are implemented. The cabin temperature can reach the reference temperature in a short period, while the lithium-ion battery temperature are robust to variations of cabin temperature. The compressor speed and the FDV opening degree are shown in Fig. 7(e) and (f). Since the initial temperatures of the lithium-ion battery and the cabin are higher than the reference temperatures, the compressor operated at maximum speed at the start of the simulation. At 900 seconds, the cabin reference temperature decreased, and the compressor speed increased to lower the cabin temperature. Overall, the ITMS simulation results align with the actual operating conditions of the vehicle.

5 CONCLUSION

In order to address the thermal management issues of FCEV, an ITMS is proposed in this paper. To tackle the control challenges of the TMS under high-temperature conditions, a Model Predictive Controller is designed. The simulation results demonstrate that the temperatures of the motor, PEMFC, lithium-ion battery, and the cabin have fast tracking ability, with lithium-ion battery response time of 2324s and cabin response time of 60.13s, fulfilling the design requirements of the ITMS. Moreover lithium-ion battery temperature is robust to variations of cabin temperature.

ACKNOWLEDGEMENT

This work is supported by International Exchange Program for Graduate Students, Tongji University.

REFERENCE

[1]Tang X, Yang M, Shi L, Hou Z, Xu S, Sun C. Adaptive state-of-health temperature sensitivity characteristics for durability improvement of PEM fuel cells. Chemical Engineering Journal. 2024;491.

[2]Song K, Ding Y, Hu X, et al. Degradation adaptive energy management strategy using fuel cell state-of-health for fuel economy improvement of hybrid electric vehicle[J]. Applied Energy, 2021, 285: 116413.

[3]Su C, Yuan X, Yu M, Bargal MHS, Tao Q, Li J, et al. Thermal Management System Modeling and Simulation of a Full-Powered Fuel Cell Vehicle. Journal of Energy Resources Technology. 2020;142.

[4]Xu J, Zhang C, Fan R, Bao H, Wang Y, Huang S, et al. Modelling and control of vehicle integrated thermal management system of PEM fuel cell vehicle. Energy. 2020;199.

[5]Lee H-S, Won J-P, Cho C-W, Kim Y-C, Lee M-Y. Heating performance characteristics of stack coolant source heat pump using R744 for fuel cell electric vehicles. Journal of Mechanical Science and Technology. 2012;26:2065-71.

[6]Wang E, Guo D, Yang F. System design and energetic characterization of a four-wheel-driven series–parallel hybrid electric powertrain for heavy-duty applications. Energy Conversion and Management. 2015;106:1264-75.

[7]Pei Y, Chen F, Jiao J, Liu S. Analysis and control strategy design for PEMFC purging process. Energy. 2024;290.

[8]Pei Y, Chen F, Jiao J, et al. Fuel cell temperature control based on nonlinear transformation mitigating system nonlinearity. Renewable Energy. 2024;230.

[9]Huang Y, Khajepour A, Bagheri F, Bahrami M. Modelling and optimal energy-saving control of automotive air-conditioning and refrigeration systems. Proceedings of the Institution of Mechanical Engineers, Part D: Journal of Automobile Engineering. 2016;231:291-309.

[10]Xu B, Arjmandzadeh Z. Parametric study on thermal management system for the range of full (Tesla Model S)/ compact-size (Tesla Model 3) electric vehicles. Energy Conversion and Management. 2023;278.